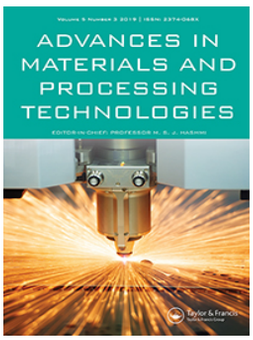

Advances in Materials and Processing Technologies

ISSN: 2374-068X (Print) 2374-0698 (Online) Journal homepage: https://www.tandfonline.com/loi/tmpt20

Thermomechanical analysis of the draw bead test

D.M. Neto, M. Pais, M.C. Oliveira, J.L. Alves & L.F. Menezes

To cite this article: D.M. Neto, M. Pais, M.C. Oliveira, J.L. Alves & L.F. Menezes (2019) Thermomechanical analysis of the draw bead test, Advances in Materials and Processing Technologies, 5:3, 401-417, DOI: 10.1080/2374068X.2019.1616478

To link to this article: https://doi.org/10.1080/2374068X.2019.1616478

Published online: 17 May 2019.

ADVANCES IN MATERIALS AND PROCESSING TECHNOLOGIES
2019, VOL. 5, NO. 3, 401–417
https://doi.org/10.1080/2374068X.2019.1616478

Taylor & Francis
Taylor & Francis Group

Thermomechanical analysis of the draw bead test

D.M. Neto[a], M. Pais[b], M.C. Oliveira[a], J.L. Alves[b] and L.F. Menezes[a]

[a]CEMMPRE, Department of Mechanical Engineering, University of Coimbra, Coimbra, Portugal; [b]CMEMS, Microelectromechanical Systems Research Unit, University of Minho, Guimarães, Portugal

ABSTRACT

Advanced high strength steels (AHSS) are currently used in stamping processes due to their good strength-to-weight ratio. However, their high strength requires improved knowledge concerning the heat generated by plastic deformation and contact with friction, since this can be an important factor for the accurate simulation of the forming process. The main objective of this study is the thermomechanical simulation of the draw bead test, with particular focus on the temperature rise. In addition to the heat generated by plastic deformation and friction, the finite element model takes into account both the heat losses to the tools and for the environment. The effects of the main process parameters are analysed, in particular, the draw bead penetration, side clearance, the pulling speed of the grip and the coefficient of friction. The results show that the parameter with the largest influence on the blank temperature is the pulling speed of the grip, which dictates the process time and consequently the heat losses by convection and contact. Although the coefficient of friction presents a strong impact on the contact forces, its influence on the temperature is negligible.

ARTICLE HISTORY
Accepted 6 May 2019

KEYWORDS
Draw bead test; numerical simulation; thermomechanical analysis; heat generation; temperature

1. Introduction

Sheet metal forming processes are widely used in the automotive industry due to the high production rates, in addition to the high quality of the produced components. Although the tools manufacturing cost can be very expensive [1], it is distributed over millions of components, allowing to obtain cheap parts. The contact conditions at the sheet–tool interface play a critical role in the forming processes. From the mechanical point of view, the frictional contact between the forming tools and the blank affects significantly both the formability and the tools wear [2]. In order to reduce the frictional forces, different lubricants have been studied, including self-lubricant coatings applied to the tools [3]. Nevertheless, the increased adoption of advanced high strength steels (AHSS) in the automotive industry leads to new challenges in the sheet metal forming operations [4]. The temperature rise at the blank and the tool surfaces can be significant due to the high contact pressures (and consequently the frictional forces) required to form these materials. In addition, the heat generated by plastic deformation is substantial due to the high strength of the AHSS materials. In fact, recent studies

CONTACT D.M. Neto diogo.neto@dem.uc.pt CEMMPRE, Department of Mechanical Engineering, University of Coimbra, Polo II, Rua Luís Reis Santos, Coimbra 3030-788, Portugal

show that temperature rises about 90–120°C are common in production conditions for these materials [5]. Therefore, the study of the temperature rise in 'cold' forming is required to improve the forming process conditions.

The draw bead test was designed to determine the friction coefficient between a metallic sheet and the deep drawing tools [6], allowing the determination of the ideal lubricant for each forming process [7]. Nevertheless, it can be adopted to analyse the heat generated by plastic deformation and frictional contact. The main objective of this study is the thermomechanical analysis of the draw bead test, using finite element simulation. Different process conditions are assessed, where the bead penetration, the side clearance, the pulling speed and the friction coefficient are studied by numerical simulation. The presented model takes into account the heat generated by plastic deformation and frictional contact, as well as the heat loss by free convection and through contact conductance. The temperature rise is evaluated for different process conditions, allowing to identify the more important parameters.

The organization of the paper considers the following sections. The setup of the draw bead test is described in Section 2, including the dimensions. The proposed finite element model is presented in Section 3, which considers the thermomechanical coupling with a staggered algorithm. The heat generated by plastic deformation and frictional forces is taken into account, as well as the heat loss by free convection and contact conductance. The comparison of different process conditions is presented in Section 4, highlighting the influence of each parameter on the temperature rise. The main conclusions of this study are outlined in Section 5.

2. Draw bead test

The draw bead test was proposed by Nine [6] to evaluate the coefficient of friction between the sheet and the tools in order to determine the ideal lubricant. This test requires four cylinders (bead, shoulders and support), which are positioned to induce plastic deformation on a metallic sheet, as illustrated in Figure 1. In the present study, all the cylinders present the same dimension (R= 10.5 mm), while the dimensions of the blank sheet are 450

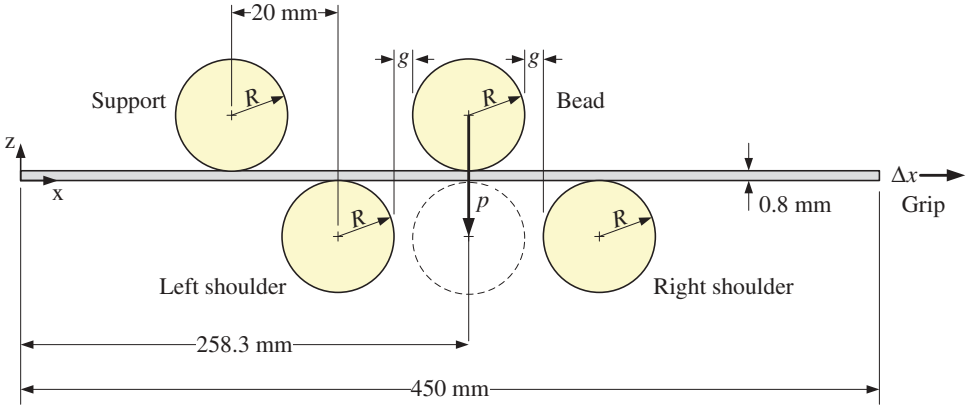

Figure 1. Scheme of the draw bead test (initial position), including the geometrical dimensions. The bead penetration is denoted by p while the horizontal grip displacement is denoted by Δx.

×25 ×0.8 mm, as schematically shown in Figure 1. The test is divided into two stages: (i) bending of the sheet by the bead and (ii) pulling of the sheet by a grip. The first stage comprises the vertical movement of the bead in order to create a penetration p over the shoulders (see Figure 1). After the bead penetration, a grip displacement (Δx) is imposed in the horizontal direction (150 mm), while the bead position is kept stationary. The pulling speed is assumed constant during this second stage.

In this study, the position of the bead along the x-direction is assumed fixed (258.3 mm), while the position of both shoulders (left and right) is adjusted from the location of the bead, defining the side clearance g. Besides, the horizontal distance between the support cylinder and the left shoulder is assumed constant (see Figure 1). Previous studies indicate that this distance is rather irrelevant in the draw bead test. In order to compare different process conditions for this test, some parameters are changed in the numerical analysis, such as the bead penetration, the side clearance, the pulling speed and the lubrication conditions (different coefficients of friction).

3. Finite element model

The numerical simulations were carried out with the in-house static finite element code DD3IMP [8], which has been continuously developed for sheet metal forming simulation. Since the aim of the study is assessing the temperature rise due to plastic deformation and frictional contact, the thermomechanical analysis of the process is mandatory. However, the effect of the temperature on the material mechanical behaviour is not taken into account, i.e. the thermomechanical coupling is assumed unidirectional, which is performed through a staggered algorithm proposed in [9]. The evolution of the blank deformation is described by an updated Lagrangian scheme. In order to take into account the heat generated by plastic deformation and friction [10], as well as the cooling of the blank induced by free convection and contact with the cylinders, the transient thermal problem is adopted in the draw bead test analysis.

3.1. Heat transfer

The differential equation that defines the thermal conduction within a solid body derives from the first law of thermodynamics coupled with Fourier's heat conduction law, which assumes the following form:

$$\rho c \frac{\partial T}{\partial t} - k\left(\frac{\partial^2 T}{\partial x^2} + \frac{\partial^2 T}{\partial y^2} + \frac{\partial^2 T}{\partial z^2}\right) - \dot{q}_{\mathrm{p}} - \dot{Q}_{\mathrm{f}} = 0, \tag{1}$$

where ρ is the mass density, c is the specific heat capacity and k is the thermal conductivity. The thermal properties of the dual phase steel DP780 are presented in Table 1. The term $\dot{q}_{\mathrm{p}}$ denotes the thermal power generated by plastic deformation, which is usually defined as the fraction of plastic power $\dot{w}^{\mathrm{p}}$ converted into heat:

$$\dot{q}_{\mathrm{p}} = \beta \dot{w}^{\mathrm{p}} = \beta(\boldsymbol{\sigma} : \dot{\boldsymbol{\varepsilon}}^{\mathrm{p}}), \tag{2}$$

where β is called the Taylor–Quinney factor [11], which is generally assumed constant and close to 0.9, $\boldsymbol{\sigma}$ is the Cauchy stress tensor and $\dot{\boldsymbol{\varepsilon}}^{\mathrm{p}}$ is the plastic strain rate tensor.

Table 1. Thermal properties of the dual phase steel DP780 [12].

Property	Value
Mass density, ρ	7858 kg/m^3
Specific heat capacity, c	442 J/(kg·K)
Thermal conductivity, k	42.3 W/(m·K)

Regarding the thermal power generated by the frictional contact between the blank and the cylinders, it can be expressed as:

$$\dot{Q}_{\mathrm{f}} = \eta(\xi\, \mathbf{t}_{\mathrm{t}} \cdot \dot{\mathbf{g}}_{\mathrm{t}}), \tag{3}$$

where ξ represents the fraction of frictional power converted into heat (100% in the present study), $\mathbf{t}_{\mathrm{t}}$ is the frictional force and $\dot{\mathbf{g}}_{\mathrm{t}}$ denotes the relative tangential slip velocity at the contact interface. The heat generated is partitioned between the two contacting bodies, where the parameter η defines the amount of heat dissipated to the blank. Although only the temperature of the blank is affected by frictional heat generation (isothermal cylinders), in this study η= 0.5.

The transient heat conduction phenomenon is expressed by Eq. (1), which involves a temperature field dependent on the time. The boundary conditions are defined on the body surface, which comprises both the free convection and the contact conductance. These conditions are defined by:

$$\dot{q}_{\mathrm{conv}} = h_{\mathrm{conv}}(T - T_{\infty}), \tag{4}$$

$$\dot{q}_{\mathrm{c}} = h_{\mathrm{c}}(T - T_{\mathrm{obs}}), \tag{5}$$

where T_{∞} and T_{obs} are the environment and isothermal obstacle temperatures. The heat transfer coefficient in free convection is denoted by h_{conv}, while the interfacial heat transfer coefficient is h_{c}.

Applying the principle of virtual temperatures to Eq. (1) and performing spatial discretization of the solid body, the matrix form of the transient heat conduction problem is given by:

$$\mathbf{C}\dot{\mathbf{T}} + \mathbf{K}\mathbf{T} = \mathbf{Q} + \mathbf{f}, \tag{6}$$

where $\mathbf{C}$ is the capacity matrix and $\mathbf{K}$ is the conductivity matrix. $\mathbf{Q}$ denotes the vector of nodal heat flux, while the vector $\mathbf{f}$ represents the prescribed heat flows and the boundary terms resulting from the environment and the contact with the isothermal obstacle. The integration of Eq. (6) over time is performed by the generalized trapezoidal method, currently implemented in the DD3IMP finite element code [9].

Considering the experimental set-up of the draw bead test, the heat loss to the environment occurs by free convection (vertical plate, since the equipment is adapted to a tensile test machine, i.e. the blank is positioned vertically). Since the pulling speed is relatively low (maximum of 20 mm/s), laminar flow conditions are assumed, where the average heat transfer coefficient, which is involved in Eq. (4), is given by [13]:

$$\bar{h} = \frac{\overline{Nu}_L \cdot k}{L}, \tag{7}$$

where $\overline{Nu}_L$ is the average Nusselt number, k is the thermal conductivity of the fluid (air) and L represents the average length of heat transfer area, which is assumed 259.5 mm based on the set-up conditions. For laminar free convection on vertical surfaces, the Nusselt number is given by:

$$\overline{Nu}_L = 0.68 + \frac{0.670 Ra_L^{1/4}}{\left(1 + (0.492/Pr)^{9/16}\right)^{4/9}}, \tag{8}$$

where Pr denotes the Prandtl number and Ra_L is the Rayleigh number, which for a laminar flow within a vertical plate is given by:

$$Ra_L = \frac{g_a \delta (T_s - T_\infty) L^3}{\alpha \nu}, \tag{9}$$

where g_a is the gravitational acceleration, δ is the volumetric thermal expansion coefficient, T_s is the blank surface temperature, T_∞ is the environment temperature, α is the thermal diffusivity, L is the average length of the heat transfer area and ν is the kinematic viscosity.

Considering the values listed in Table 2 and assuming a temperature difference between the blank and the air of 10 K (unknown *a priori*), the Rayleigh number defined in Eq. (9) is 1.5×10^7. This value is inferior to the one defining the transition to the turbulent regime (10^9), confirming the laminar flow conditions. Accordingly, the average Nusselt number calculated for these conditions is 32.7. Finally, the obtained value for the heat transfer coefficient in free convection is $h_{conv} = 3.4$ W/m^2·K.

Despite the heat loss to the environment through free convection, the mechanical contact between the blank and the cylinders leads to an important heat loss by contact conductance. From the numerical point of view, this heat loss is usually modelled as convection (see Eq. (5)), taking place on the contact interface, where the interfacial heat transfer coefficient is the main parameter. This parameter depends significantly on several factors, such as temperature, contact pressure, surface roughness, material properties[14,15]. Nevertheless, the experimental evaluation of this parameter requires a dedicated device. Thus, based on the tabulated values for two identical metal surfaces (steel) with air at the interface and contact pressures ranging between 0.2 and 7 MPa [13], the interfacial heat transfer coefficient is 3100 W/m^2·K.

In order to take into account the dependence of the interfacial heat transfer coefficient on several factors, the model proposed by Martins [10] is adopted in the present

Table 2. Properties of the air (at 303 K) used to evaluate the heat transfer coefficient in free convection [12].

Property	Value
Volumetric thermal expansion coefficient, δ	3.3×10^{-3} K^{-1}
Prandtl number, Pr	0.727
Thermal diffusivity, α	2.29×10^{-5} m^2/s
Kinematic viscosity, ν	1.62×10^{-5} m^2/s
Thermal conductivity, k	2.65×10^{-2} W/(m·K)
Average length of the heat transfer area, L	259.5 mm

study. This model allows for obtaining a smooth variation of the heat transfer coefficient between contact and non-contact (free convection) areas. Accordingly, the interfacial heat transfer coefficient is dependent on the gap distance between contacting bodies, which is given by:

$$h_c = h_{sup} \exp(-m g_n), \tag{10}$$

where h_{sup} the upper threshold value (in contact) and m is a free parameter used to control the rate of decrease with the gap distance g_n. In the present study, this parameter is adjusted to fit the heat transfer coefficient in free convection, when the gap distance reaches 1 mm. Figure 2 presents the variation of the interfacial heat transfer coefficient with the gap distance, highlighting the value of 3.4 W/m^2·K when the gap distance reaches 1 mm.

3.2. Material mechanical behaviour

The dual phase steel DP780 is the material adopted in this study for the blank. The mechanical behaviour is assumed elastoplastic, considering isotropic elastic behaviour and anisotropic plastic behaviour. The elastic behaviour is described by the Hooke's law with a Young's modulus of 210 GPa and a Poisson's ratio of 0.30. Regarding the plastic behaviour, the hardening is described by the Swift's law:

$$Y = K(\varepsilon_0 + \bar{\varepsilon}^p)^n, \tag{11}$$

where K, ε_0, and n are the material parameters, while $\bar{\varepsilon}^p$ denotes the equivalent plastic strain. The material parameters are identified by the least squares fitting using the experimental stress–strain curve from the uniaxial tensile test carried out in the rolling direction. The obtained material parameters for the Swift's hardening law are listed in Table 3. The comparison between experimental and numerical work hardening is presented in Figure 3 (a), highlighting the accuracy of the adopted constitutive model to describe the mechanical behaviour of this steel. Due to the lack of experimental results, the mechanical behaviour of this steel is assumed temperature and strain rate independent.

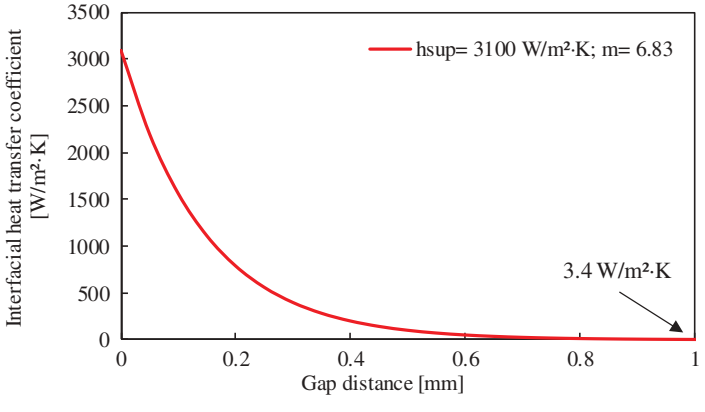

Figure 2. Variation of the interfacial heat transfer coefficient as a function of the normal distance to the isothermal surface.

Table 3. Material parameters used to define the isotropic hardening (Swift law) of the DP780 steel. Y_0 denotes the yield stress according to the Swift law.

Material	Y_0 [MPa]	K [MPa]	ε_0	n
DP780	500.7	1319.21	0.0015	0.1490

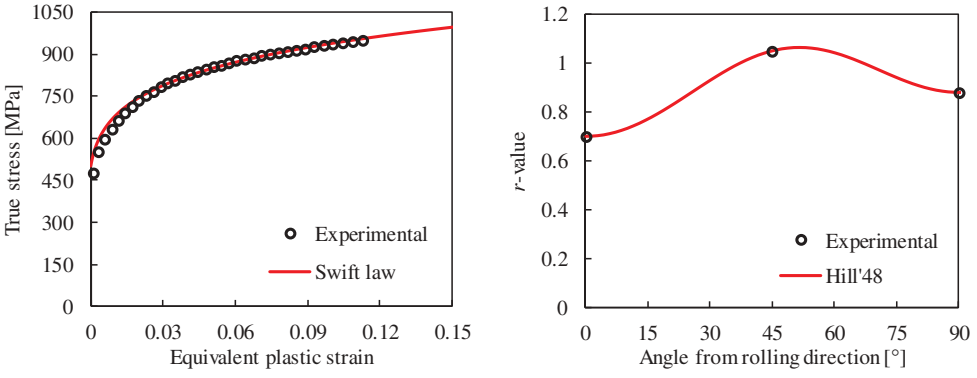

Figure 3. Comparison between experimental and numerical predictions for the anisotropic plastic behaviour of the DP780 steel: (a) True stress–strain curve obtained from the uniaxial tensile test (specimen aligned with the rolling direction); (b) evolution of the coefficient of anisotropy (*r*-value) in the plane of the sheet.

Regarding the plastic anisotropic behaviour of the DP780 steel, it is described by the Hill'48 yield criterion. The anisotropy parameters are determined from experimental *r*-values, evaluated through uniaxial tensile tests performed at three different angles with respect to the rolling direction: 0º, 45º and 90º (see Table 4). Since the identification of the hardening law parameters was carried out using specimens oriented along the rolling direction, the relation $G+H=1$ is added. The obtained anisotropy parameters of the Hill'48 yield criterion are presented in Table 5. The comparison between experimental and predicted anisotropy coefficient in-plane distributions is presented in Figure 3(b).

Table 4. Anisotropy coefficients (*r*-values) experimentally evaluated at different angles with respect to the rolling direction.

Material	r_0	r_{45}	r_{90}
DP780	0.70	1.05	0.88

Table 5. Hill'48 anisotropy parameters calculated for the DP780 steel.

Material	F	G	H	L	M	N
DP780	0.468	0.588	0.412	1.500	1.500	1.637

3.3. Blank and tools discretization

The blank is discretized with linear hexahedral finite elements, adopting the same finite element mesh (structured) in the mechanical and thermal problem [16], avoiding the application of remapping methods. Nevertheless, full integration is adopted in the thermal problem, while the mechanical problem resorts to the selective reduced integration technique [17] to avoid volumetric locking. For a blank width of 25 mm, the deformation is negligible along this direction, allowing to assume plane strain conditions. On the other hand, three layers of finite elements are adopted in the thickness direction in order to capture accurately the through-thickness gradients. The zone of the blank that will be in contact with the cylinders during the test is discretized with small finite elements (0.26 mm in the length direction to approximate a unitary ratio between both finite element dimensions [18]).

The cylinders are considered perfectly rigid in the finite element model, which are modelled by Nagata patches [19]. Each cylindrical surface is described by 60 Nagata patches, as shown in Figure 4. The friction between the blank and the cylinders is defined by the classical Coulomb friction law. Although the mechanical contact between the blank and the cylinders occurs only in specific regions, the entire geometry of the tools is modelled, since it can be important for the thermal conditions. The cylinders are assumed isothermal bodies, presenting the room temperature during the test.

4. Results and discussion

This section contains the numerical results of the draw bead test, comparing different process conditions, such as bead penetration, side clearance, pulling speed and friction coefficient. This sensitivity analysis is performed considering the reference the model with: (i) 21.8 mm of bead penetration (full penetration); (ii) 1.2 mm of side clearance; (iii) 1 mm/s of pulling speed and (iv) friction coefficient of 0.15.

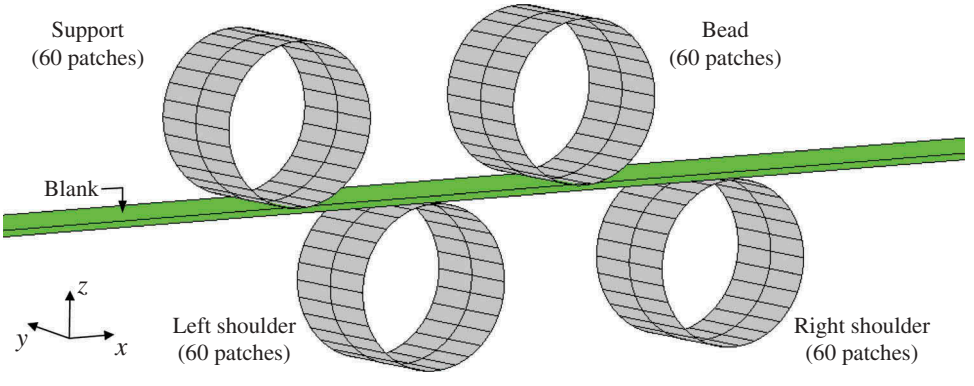

Figure 4. Discretization of the cylinders using Nagata patches. Location of the blank at the beginning of the draw bead test.

4.1. Bead penetration

This section contains the influence of the bead penetration on the predicted forces, temperature distribution and contact angles. Three different values of bead penetration are adopted in the numerical model, namely 21.8 mm, 16.35 mm and 10.9 mm, which correspond to full penetration, 75% of the penetration and 50% of the penetration, respectively. All other process conditions (side clearance, pulling velocity and friction coefficient) are assumed with the reference value.

The evolution of the bead force in the z-direction is presented in Figure 5 (a) for three different values of bead penetration. The force evolution is the same for all conditions, changing only the maximum value attained, which is dictated by the penetration value. Thus, large values of bead force occur for the higher values of penetration. The evolution of the bead force during the grip displacement is presented in Figure 5 (b). The force increases quickly (about 15%) at the beginning of the grip displacement and then reaches a steady state regime for grip displacement higher than 50 mm, as shown in Figure 5(b). The maximum bead force value occur for full penetration, which is about 2.5 kN.

In order to quantify the contact between the blank and the cylinders, three contact angles are defined, θ_1, θ_2 and θ_3, which describe the contact with the left shoulder, bead and right shoulder, respectively. These angles are obtained by considering the first and last node of the blank in contact with each cylinder, as shown in Figure 6.

The contact angles defined in Figure 6 are evaluated both during the displacement of the bead (Figure 7(a)) and during the grip displacement (Figure 7(b)). The vertical movement of the bead leads to an increase of the angle θ_2 from the beginning, while the angles θ_1 and θ_3 start to increase only when the bead displacement reaches at least 10.9 mm. The maximum values are obtained considering full bead penetration conditions, which are about 34°, 150° and 60°, for θ_1, θ_2 and θ_3, respectively. After a slight decrease, these contact angles tend to stabilize during the displacement of the grip, a consequence of the steady state regime achieved.

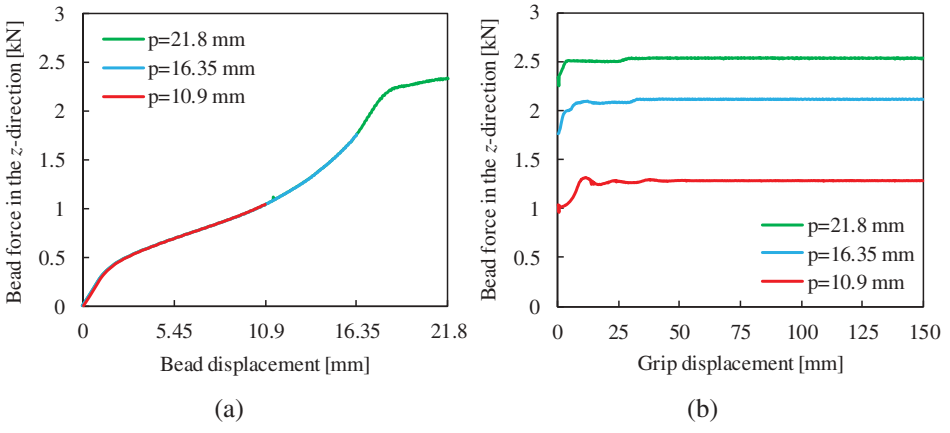

Figure 5. Evolution of the bead force in the z-direction for the three different values of bed penetration: (a) during bead displacement; (b) during grip displacement.

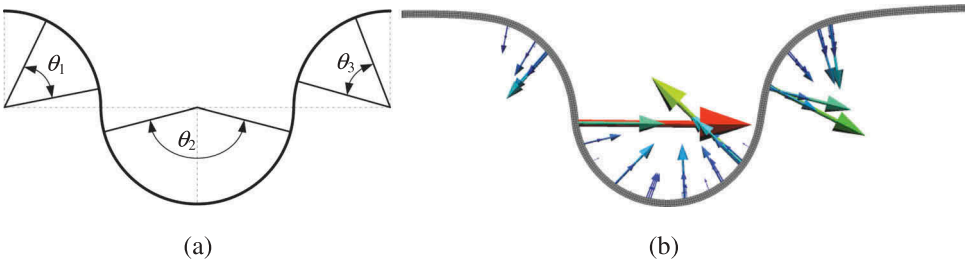

Figure 6. Definition of the angles, θ_1, θ_2 and θ_3: (a) schematic approach; (b) nodal contact forces for full bead penetration conditions.

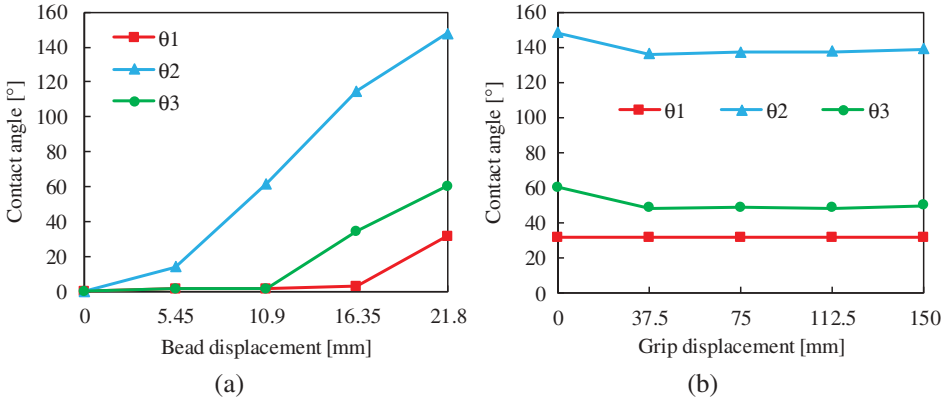

Figure 7. Evolution of contact angles, θ_1, θ_2 and θ_3 for full penetration condition: (a) during bead displacement; (b) during grip displacement.

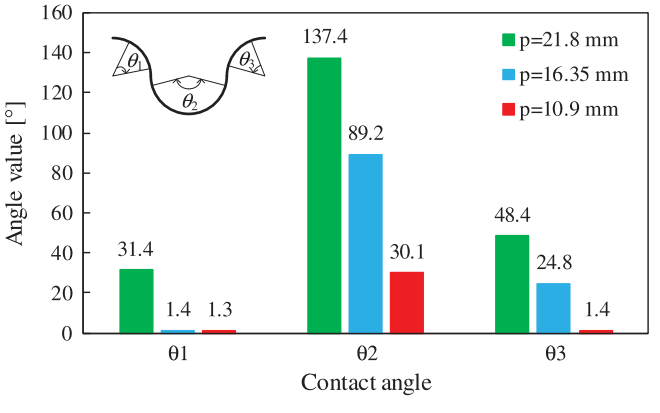

Figure 8. Influence of the bead penetration on the contact angles θ_1, θ_2 and θ_3, measured at a grip displacement of 112.5 mm (steady state regime).

The influence of bead penetration on the contact angles, θ_1, θ_2 and θ_3, is presented in Figure 8, which contains the angle values observed in the steady-state regime (112.5 mm of grip displacement). The large values of contact angles arise for full penetration conditions. Besides, the contact angle θ_1 is always the lower one, while

the angle θ_2 is the largest one. The difference between θ_1 and θ_3 results from the applied boundary conditions, i.e. the pulling is applied on the right side of the sheet. Moreover, the contact angles θ_1 and θ_3 are very small for the lower value of bead penetration (see Figure 8), indicating a local contact situation.

The flow of the sheet between the cylinders induces plastic deformation, which leads to a temperature rise on the sheet. The equivalent plastic strain and the temperature distribution are shown in Figure 9, evaluated at the end of the pulling stage for three different values of bead penetration. The maximum temperature rise occurs for the lower penetration value, which induces lower plastic strain values. Although the heat energy generated by plastic deformation is lower, the heat loss to the cylinders by contact conductance is considerably lower, because it is proportional to the contact areas (see Figure 8). Therefore, the contact angles present a strong influence on the temperature rise. Indeed, for the full penetration case, the temperature rise is the lowest of the three cases.

4.2. Side clearance

The influence of the side clearance (see Figure 1) on the process results is evaluated in this section. Four values of side clearance are adopted in the finite element model, namely 0.8 mm, 1.0 mm, 1.2 mm and 1.6 mm, which means a range between the initial thickness of the blank and 200% of its value. The evolution of the bead force in the z-direction is presented in Figure 10(a) for four different values of side clearance. The force evolution is similar in all cases until approximately 15 mm of bead penetration. Then, the force increases significantly for the lower value of clearance. The evolution of the bead force in the z-direction during the grip displacement is presented in Figure 10(b). The higher force value occurs for the lower side clearance, as expected. Nevertheless, the influence of the side clearance on the bead force is relatively small, except when the side clearance is exactly the initial thickness of the blank, as shown in Figure 10.

Concerning the influence of the side clearance on the contact angles, Figure 11 presents the contact angles values for the four-side clearances adopted in this study. The angles θ_1, θ_2 and θ_3 increase with the decrease of the side clearance, since the bead becomes increasingly embraced

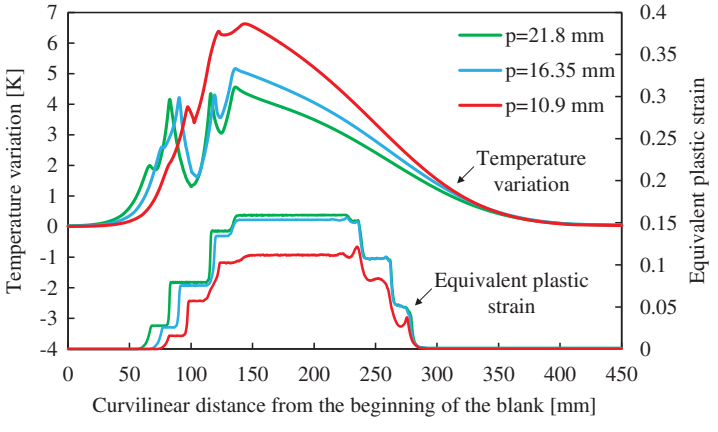

Figure 9. Influence of the bead penetration on both the temperature and the equivalent plastic strain distributions obtained at the end of the pulling.

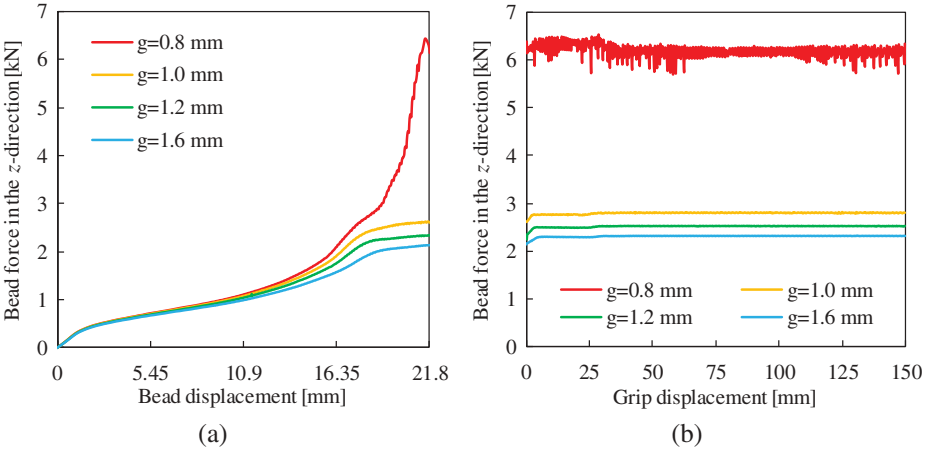

Figure 10. Evolution of the bead force in the *z*-direction for four different values of side clearance: (a) during bead displacement; (b) during grip displacement.

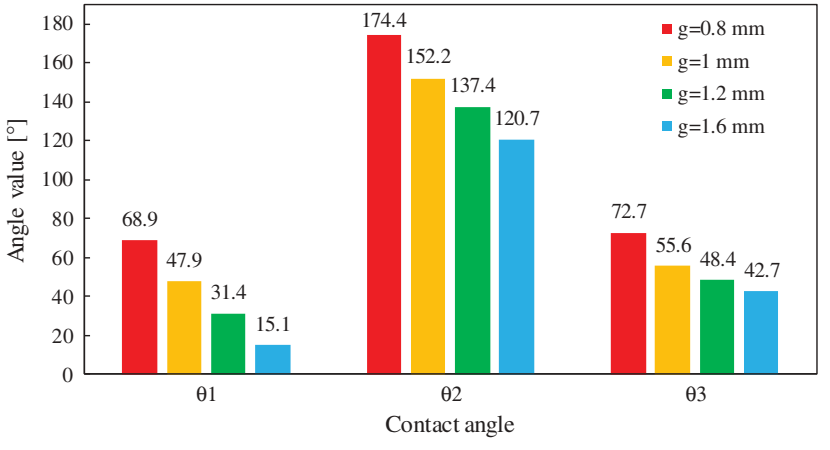

Figure 11. Influence of the side clearance on the contact angles θ_1, θ_2 and θ_3, measured at a grip displacement of 112.5 mm (steady state regime).

by the blank when the left and right shoulders reduce their distance to the bead. In fact, for g= 0.8 mm, the overall contact angle (θ_1+ θ_2+ θ_3) is close to the wrap angle (360°) considered by Nine [6] to evaluate the friction coefficient. The angle most affected by this clearance is θ_1, as shown in Figure 11. The study carried out by Oliveira et al. [20] highlights the discrepancy in the friction coefficient evaluated using Nine's model, which results from this difference in the contact angle and the non-uniform contact pressure.

Figure 12 presents the distribution of the temperature rise at the end of the grip displacement, comparing four values of side clearance. The maximum temperature rise occurs for the lowest side clearance values due to the larger value of plastic strain attained. Regarding the localization, it arises between the left shoulder and the bead, as well as between the right shoulder and the bead. Nevertheless, the temperature gradient in these locations is very high, as highlighted in Figure 12. On the other hand, the

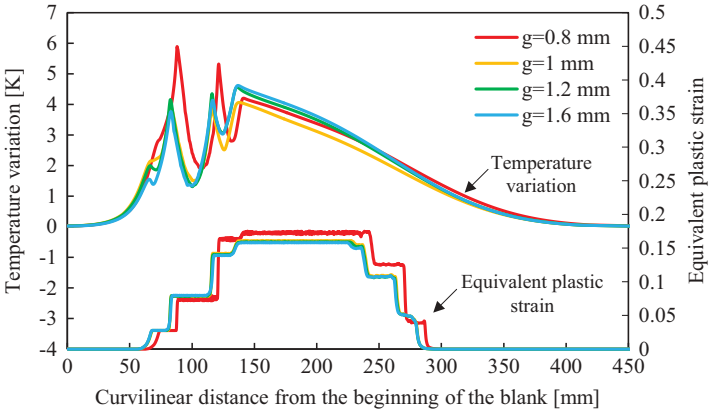

Figure 12. Influence of the side clearance on both the temperature and the equivalent plastic strain distributions obtained at the end of the pulling.

temperature distribution at the exit of the right shoulder presents a reduced gradient during a length longer than 50 mm. Since the plastic strain is identical for all values of side clearance, except for the smaller one, the temperature rise is lower for large values of contact area with the cylinders (Figure 11), which imposes more heat losses (see Figure 12).

4.3. Pulling speed

In order to assess the effect of the pulling velocity on the predicted temperature, three values are considered in the numerical model, namely 1 mm/s, 10 mm/s and 20 mm/s. Since the thermomechanical coupling is unidirectional, i.e. the mechanical behaviour is independent of the temperature; the change of the pulling speed only affects the temperature evolution. The thermal power generated by plastic deformation, defined in Equation (2), which is mainly responsible by the temperature rise, increases with the

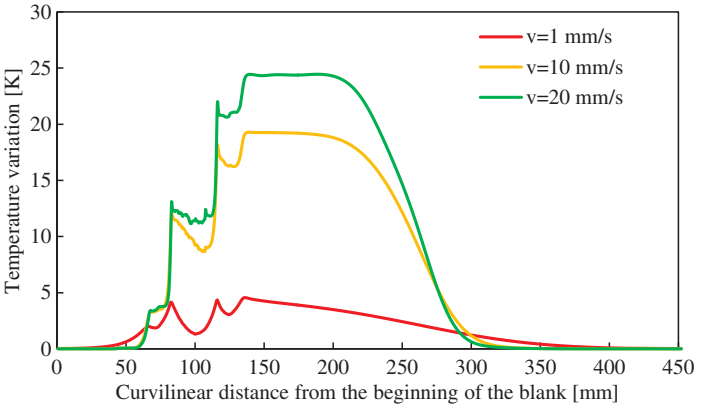

Figure 13. Influence of the pulling speed on the temperature distribution obtained at the end of the pulling.

pulling velocity due to the strain rate increase. Nevertheless, the total time of the test reduces with the increase of the pulling velocity.

Figure 13 presents the temperature distribution predicted at the end of the pulling, considering three pulling velocities. The temperature of the blank increases with the pulling speed because the time available for the heat loss to the cylinders and the environment is lower. Increasing the pulling speed from 1 mm/s to 10 mm/s, the maximum temperature achieved increases approximately 15 K, highlighting the large influence of the pulling speed on the temperature rise. Since the heat losses to the environment and to cylinders are time-dependent, the overall blank temperature increases due to the less time for heat transfer from the blank.

4.4. Friction coefficient

The influence of the friction coefficient μ on the predicted results is studied, considering five values of friction coefficient, specifically 0.00, 0.05, 0.10, 0.15 and 0.20. The evolution of the bead force in the z-direction is presented in Figure 14, both during the bead penetration and during the grip displacement. The increase in the friction coefficient leads to a consequent increase in the contact forces. Indeed, considering the steady-state regime, the bead force increases from about 1.6 kN under frictionless conditions up to 2.9 kN for μ= 0.2.

The influence of the friction coefficient on the pulling force during the grip displacement is presented in Figure 15. This force increases suddenly at the beginning and then achieves the steady-state regime, where the force is approximately constant. The magnitude of this force is slightly higher than the one observed for the bead (z-direction). The force magnitude increases about 20% for each increment of μ, from 1.69 kN (frictionless case) to 3.65 kN obtained for the friction coefficient of 0.2.

Figure 16 presents both the equivalent plastic strain and the temperature distribution, evaluated at the end of the pulling stage for different values of friction coefficient. Since the effect of the friction coefficient on the plastic strain is negligible, the temperature increase is similar in all conditions. The largest difference in the predicted temperature occurs between the frictionless and μ= 0.2 cases, which is lower than 0.4°.

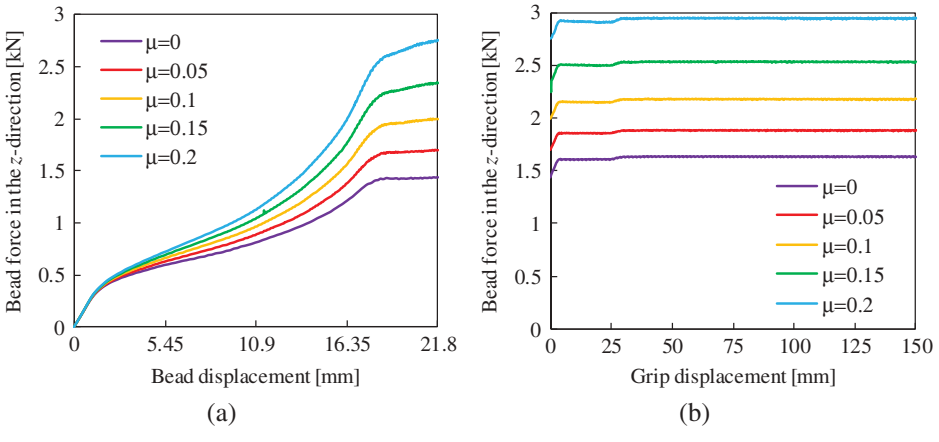

Figure 14. Evolution of the bead force in the z-direction for different values of friction coefficient: (a) during bead displacement; (b) during grip displacement.

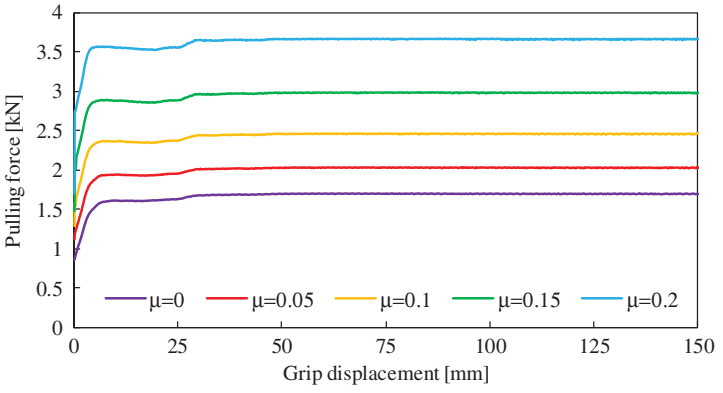

Figure 15. Influence of the friction coefficient on the pulling force evolution.

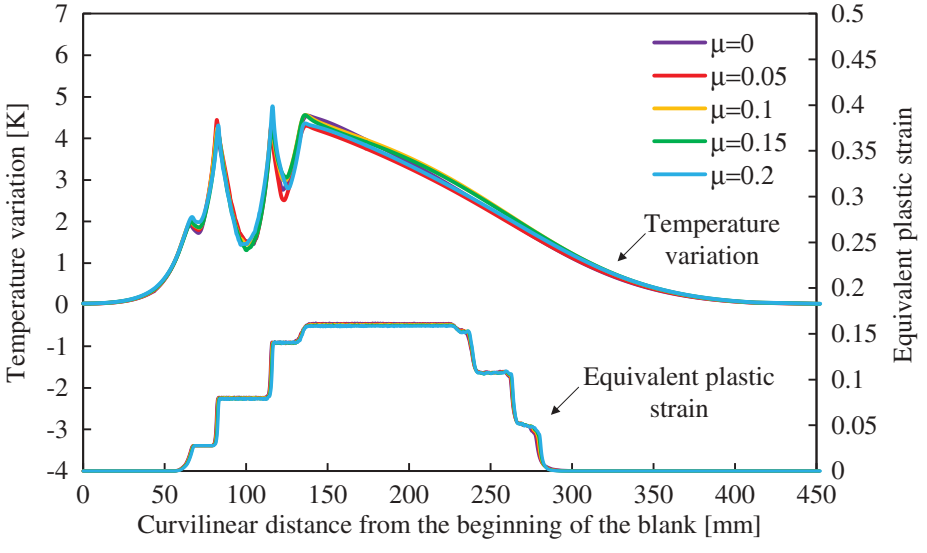

Figure 16. Influence of the friction coefficient on both the temperature and the equivalent plastic strain distributions obtained at the end of the pulling.

Thus, the heat generated by frictional sliding can be considered negligible in comparison with the one generated by plastic deformation.

5. Conclusions

The adoption of advanced high strength steels in sheet metal forming processes is increasing due to their good strength-to-weight ratio. However, large contact pressures and forming forces arise due to the high strength of these materials. Thus, improved knowledge concerning the heat generated by friction and plastic deformation is required, which is important for the accurate process simulation. This study presents the thermo-mechanical analysis of the draw bead test, considering the dual phase steel DP780.

The proposed finite element model takes into account both the heat generated by plastic deformation and friction, as well as the heat losses to the environment by free convention and the contact conductance with the forming tools. The cylinders of the draw bead test are assumed rigid and isothermal, while the blank presents an elasto-plastic behaviour. Different process conditions are analysed, namely the bead penetration, side clearance, pulling speed and friction coefficient. The effect of these parameters on the temperature rise is evaluated.

Although the contact forces are strongly influenced by the coefficient of friction, its influence on the temperature rise is negligible. Therefore, the heat generated by the friction forces during the sliding is significantly lower than the one resulting from the plastic deformation. In fact, the temperature rise is predominantly influenced by the pulling speed, due to the change of the process time available for the occurrence of heat losses (environment and cylinders). Regarding the bead penetration, the temperature rises when the penetration is lower due to the reduced contact area, which reduce the heat loss through contact conductance.

Acknowledgments

The authors greatly appreciate the helpful contribution of Prof Abel Santos on the experimental mechanical characterization of the adopted steel. The first author is also grateful to the Fundação para a Ciência e a Tecnologia for the Postdoctoral grant SFRH/BPD/101334/2014.

Disclosure statement

No potential conflict of interest was reported by the authors.

Funding

This work was supported by the Portuguese Foundation for Scienceand Technology (FCT) under projects FCT/INDIA, PTDC/EMS-TEC/0702/2014 (POCI-01-0145-FEDER-016779) and PTDC/EMS-TEC/6400/2014 (POCI-01-0145-FEDER-016876) by UE/FEDER through the program COMPETE 2020.

ORCID

D.M. Neto http://orcid.org/0000-0002-2296-4009
M.C. Oliveira http://orcid.org/0000-0001-8032-7262
J.L. Alves http://orcid.org/0000-0001-8714-4880
L.F. Menezes http://orcid.org/0000-0002-4703-9346

References

[1] Doege E, Elend L-E. Design and application of pliable blank holder systems for the optimization of process conditions in sheet metal forming. J Mater Process Technol. 2001;111:182–187.
[2] Lovell M, Higgs CF, Deshmukh P, et al. Increasing formability in sheet metal stamping operations using environmentally friendly lubricants. J Mater Process Technol. 2006;177:87–90.

[3] Basnyat P, Luster B, Kertzman Z, et al. Mechanical and tribological properties of CrAlN-Ag self-lubricating films. Surf Coatings Technol. 2007;202:1011–1016.
[4] Pereira MP, Rolfe BF. Temperature conditions during "cold" sheet metal stamping. J Mater Process Technol. 2014;214:1749–1758.
[5] Wagoner RH, Kim JH, Sung JH. Formability of advanced high strength steels. Int J Mater Form. 2009;2:359–362.
[6] Nine HD. Drawbead forces in sheet metal forming. In: Donald P. Koistinen and Neng-Ming Wang (eds.), Mechanics of sheet metal. Boston, MA: Springer US; 1978. p. 179–211. DOI:10.1007/978-1-4613-2880-3_8
[7] Bay N, Olsson DD, Andreasen JL. Lubricant test methods for sheet metal forming. Tribol Int. 2008;41:844–853.
[8] Menezes LF, Teodosiu C. Three-dimensional numerical simulation of the deep-drawing process using solid finite elements. J Mater Process Technol. 2000;97:100–106.
[9] Martins JMP, Neto DM, Alves JL, et al. A new staggered algorithm for thermomechanical coupled problems. Int J Solids Struct. 2017;122–123:42–58.
[10] Martins JMP, Neto DM, Alves JL, et al. Numerical modeling of the thermal contact in metal forming processes. Int J Adv Manuf Technol. 2016;87:1797–1811.
[11] Taylor GI, Quinney H. The latent energy remaining in a metal after cold working. Proc R Soc A Math Phys Eng Sci. 1934;143:307–326.
[12] Çengel YA, Ghajar AJ. Heat and mass transfer: fundamentals & applications. New York: McGraw-Hill Education; 2014.
[13] Bergman TL, Lavigne AS, Incropera FP, et al. Fundamentals of heat and mass transfer. 7th ed. New York: Wiley; 2011.
[14] Pereira MP, Yan W, Rolfe BF. Contact pressure evolution and its relation to wear in sheet metal forming. Wear. 2008;265:1687–1699.
[15] Chang Y, Tang X, Zhao K, et al. Investigation of the factors influencing the interfacial heat transfer coefficient in hot stamping. J Mater Process Technol. 2016;228:25–33.
[16] Adam L, Ponthot J-P. Thermomechanical modeling of metals at finite strains: first and mixed order finite elements. Int J Solids Struct. 2005;42:5615–5655.
[17] Hughes TJR. Generalization of selective integration procedures to anisotropic and non-linear media. Int J Numer Methods Eng. 1980;15:1413–1418.
[18] Padmanabhan R, Oliveira MC, Baptista AJ, et al., Study on the Influence of the Refinement of a 3-D Finite Element Mesh in Springback Evaluation of Plane-Strain Channel Sections. AIP Conference Proceedings, 2007; 908: 847–852.
[19] Neto DM, Oliveira MC, Menezes LF, et al. Applying Nagata patches to smooth discretized surfaces used in 3D frictional contact problems. Comput Methods Appl Mech Eng. 2014;271:296–320.
[20] Oliveira MC, Alves JL, Menezes LF, et al., Finite Element Analysis ofthe Amontons-Coulomb's Model using Local and Global Friction Tests. AIP Conference Proceedings, 2011; 1353: 1812–1817.